Type IIP supernova SN 2004et: a multiwavelength study in X-ray, optical and radio

Kuntal Misra,[1]★ Dave Pooley,[2]★† Poonam Chandra,[3,4]★ D. Bhattacharya,[5]★
Alak K. Ray,[6]★ Ram Sagar[1]★ and Walter H. G. Lewin[7]★

[1]*Aryabhatta Research Institute of Observational Sciences, Manora Peak, Nainital 263129, India*

[2]*Astronomy Department, University of California at Berkeley, Berkeley, CA 94720, USA*

[3]*National Radio Astronomy Observatory, Charlottesville, VA 22903, USA*

[4]*University of Virginia, Charlottesville, VA 22904, USA*

[5]*Raman Research Institute, Bangalore 560080, India*

[6]*Tata Institute of Fundamental Research, Homi Bhabha Road, Mumbai 400005, India*

[7]*Center for Space Research and Department of Physics, Massachusetts Institute of Technology, 70 Vassar Street, Building 37, Cambridge, MA 02139-4307,
USA*

ABSTRACT

We present X-ray, broad-band optical and low-frequency radio observations of the bright type IIP supernova SN 2004et. The *Chandra X-ray Observatory* observed the supernova at three epochs, and the optical coverage spans a period of $\sim$470 d since explosion. The X-ray emission softens with time, and we characterize the X-ray luminosity evolution as $L_X \propto t^{-0.4}$. We use the observed X-ray luminosity to estimate a mass-loss rate for the progenitor star of $\sim 2 \times 10^{-6}\, M_\odot\, yr^{-1}$. The optical light curve shows a pronounced plateau lasting for about 110 d. Temporal evolution of photospheric radius and colour temperature during the plateau phase is determined by making blackbody fits. We estimate the ejected mass of ^{56}Ni to be $0.06 \pm 0.03\, M_\odot$. Using the expressions of Litvinova & Nadëzhin we estimate an explosion energy of $(0.98 \pm 0.25) \times 10^{51}$ erg. We also present a single epoch radio observation of SN 2004et. We compare this with the predictions of the model proposed by Chevalier, Fransson & Nymark. These multiwavelength studies suggest a main-sequence progenitor mass of $\sim$20 $M_\odot$ for SN 2004et.

Key words: techniques: photometric – supernovae: general – supernovae: individual: SN 2004et.

1 INTRODUCTION

Supernovae of the type II are generally associated with regions of star formation in spiral galaxies. They are believed to result from the explosion triggered by core-collapse of massive stars, presumably red supergiants with main-sequence mass of 10–25 $M_\odot$, having a thick hydrogen envelope. Spectra of type II supernovae (SNe II) show the evidence of hydrogen near maximum light. A further differentiation is proposed for SN II based on the shape of light curve. Those which have a pronounced plateau and remain within $\sim$1 mag of maximum brightness for an extended period are termed as type IIP (plateau) while those showing a linear decline in magnitude from the peak are termed as type IIL (linear).

The plateau duration is usually between 60–100 d which is followed by an exponential tail at later epochs. The plateau phase corresponds to a period of nearly constant luminosity due to the hydrogen recombination wave receding through the envelope and it slowly releases the energy which was deposited by the shock and radioactive decay. Over the years enormous progress has been made in the study of SNe. But the detailed photometric and spectroscopic data especially for SN IIP are still rare. Also the direct determination of the progenitors has been possible due to the availability of many ground- and space-based archival images. A well-studied sample of SN IIP and their observational properties during the plateau phase will give valuable information about the range of progenitor masses, the explosion energy, the ejected mass and the amount of ejected ^{56}Ni.

In this paper, we report the *Chandra* X-ray observations, detailed optical observations and radio detection (at 1.4 GHz) of a type IIP supernova SN 2004et which occurred in the spiral starburst galaxy NGC 6946 which is located at a distance of 5.5 Mpc. Due to its proximity ($z = 0.000\,16$) was a very promising candidate to study

★E-mail: kuntal@aries.ernet.in (KM); dave@astron.berkeley.edu (DP); pc8s@virginia.edu (PC); dipankar@rri.res.in (DB); akr@tifr.res.in (AKR); sagar@aries.ernet.in (RS); lewin@space.mit.edu (WHGL)
†Chandra Fellow.

the overall evolution at different wavelengths. It was the second brightest SN (unfiltered magnitude 12.8) detected in the year 2004, the brightest being a type IIP SN 2004dj (unfiltered magnitude 11.2) in NGC 2403. The X-ray, optical photometric and radio observations of SN 2004et will make it one of the best studied SN IIP in the present era. Supplementing this is the progenitor identification of SN 2004et by Li et al. (2005) using the pre-SN images of NGC 6946 with the Canada–France–Hawaii Telescope (CFHT).

SN 2004et was discovered on 2004 September 27 by S. Moretti (Zwitter, Munari & Moretti 2004) with a 0.4-m telescope. The location of the SN, RA 20^h 35^m $25\overset{s}{.}33$ and Dec. $+60°$ $07'$ $17\overset{''}{.}3$ (J2000.0) was 247.1 arcsec east and 115.4 arcsec south of the nucleus of the galaxy NGC 6946. A high-resolution spectroscopy obtained with the 1.82-m Asiago telescope on September 28 confirmed it as a type II event and the equivalent width of Na I D II lines implied a total reddening of $E(B - V) = 0.41$ mag. Further observations were carried out by Li et al. (2004) with the 0.76-m Katzman Automated Imaging Telescope.

The TAROT robotic telescope which imaged NGC 6946 frequently found no optical source at the SN location on September 22.017. Based on these TAROT measurements Li et al. (2005) constrain the explosion date for SN 2004et as September 22.0 (JD 245 3270.5) which we have adopted as the explosion epoch in this paper.

Li et al. (2004) report that the progenitor of SN 2004et was seen as a faint, extended source on NGC 6946 images taken with 0.9-m Kitt Peak telescope on 1989 May 30 and the high-quality images taken with 3.6-m CFHT on 2002 August 6 show the presence of a possible progenitor within 0.3 arcsec of the SN 2004et position. The estimated luminosity for these is consistent with a massive supergiant but it is too bright and too blue for a single red supergiant. Li et al. (2005) present a detailed analysis of the progenitor of supernova SN 2004et and conclude that the progenitor was a yellow supergiant ($15^{+5}_{-2} M_\odot$) which might have experienced a red supergiant stage before explosion. They also mention the possibility of the progenitor being an interacting system of a red and a blue supergiant similar to the progenitor of supernova SN 1993J. SN 2004et progenitor is the seventh one which is directly identified.

SN 2004et was also detected at radio wavelengths (22.4 and 8.4 GHz) by Stockdale et al. (2004) using the Very Large Array (VLA) on October 5.128 UT. No radio emission was detected on September 30.18 UT. The radio position is in close agreement with the optical position. Beswick et al. (2004) report the radio observations at 4.9 GHz using a subset of the MERLIN array. NGC 6946 has been the galaxy most prolific at producing SN discoveries, hosting a total of eight objects (SN 1917A, SN 1939C, SN 1948B, SN 1968D, SN 1969P, SN 1980K, SN 2002hh and SN 2004et). Four of these have been detected at radio wavelengths (SN 1968D, SN 1980K, SN 2002hh and SN 2004et). SN 2004et was detected at X-ray wavelengths and was observed by *Chandra* X-ray satellite.

We have carried out the multicolour optical photometric observations of SN 2004et from ~14 to 470 d after the explosion. Radio observations of SN 2004et were carried out at a single epoch at 1.4 GHz. Section 2 briefly discusses the X-ray, optical and radio observations. Development of X-ray light curve and spectrum, optical photometric evolution and interpretation of the radio observation are discussed in the Sections 3, 4 and 7, respectively. Comparison of SN 2004et with other SNe IIP forms Section 5, X-ray emission is discussed in Section 6 whereas the conclusions form Section 8 of the paper.

2 OBSERVATIONS AND DATA REDUCTION

2.1 X-ray observations and *Chandra* data reduction

SN 2004et was observed with *Chandra* on three occasions −30, 45 and 72 d since explosion – for ~30 ks each, as part of a programme to explore the X-ray properties of core-collapse SNe (PI: Lewin); details of the observations can be found in Table 3. An initial report of the observations was made by Rho, Jarrett & Chevalier (2007). All data were taken with the Advanced CCD Imaging Spectrometer (ACIS) with an integration time of 3.2 s per frame. The telescope aimpoint was on the back-side-illuminated S3 chip, and the data were telemetered to the ground in 'faint' mode.

Data reduction was performed using the CIAO 3.3 software provided by the *Chandra X-ray Center*[1]. The data were reprocessed using the CALDB 3.2.2 set of calibration files (gain maps, quantum efficiency, quantum efficiency uniformity, effective area) including a new bad pixel list made with the acis_run_hotpix tool. The reprocessing was done without including the pixel randomization that is added during standard processing. This omission slightly improves the point spread function. The data were filtered using the standard *ASCA* grades (0, 2, 3, 4 and 6) and excluding both bad pixels and software-flagged cosmic ray events. This is the standard grade filtering for ACIS imaging observations recommended by the *Chandra X-ray Center*; this filtering optimizes the signal-to-background ratio. Intervals of strong background flaring were searched for, but none were found.

2.2 Optical observations and data analysis

We have carried out the broad-band $UBVR_cI_c$ optical photometric observations of SN 2004et at 29 epochs during 2004 October 06 to 2005 January 01. Further observations were precluded due to its proximity to the Sun. The observations were continued again in 2005 October. We could observe SN 2004et at 24 epochs during 2005 October 13 to 2006 January 05. We present, here, an extended coverage of SN 2004et at 53 epochs spanning over 470 d since the explosion on 2004 September 22. All the observations were carried out using a 2048 × 2048 CCD camera mounted at the f/13 Cassegrain focus of the 1.04-m Sampurnanand Telescope (ST) at Aryabhatta Research Institute of Observational Sciences (ARIES), Nainital. One pixel of the CCD chip corresponds to a square of 0.38 arcmin side, and the entire chip covers a field of 13 × 13 arcmin^2 on the sky. The gain and readout noise of the CCD camera are 10 electrons per analogue-to-digital unit and 5.3 electrons, respectively.

We observed the Landolt (1992) standard PG 0231+051 field and the SN in $UBVR_cI_c$ filters on 2004 November 14 for photometric calibration during good photometric sky conditions. Several bias and twilight flat frames were observed with the CCD camera to calibrate the images using standard techniques. The bias-subtracted, flat-fielded and cosmic ray removed images were used for further analysis.

Image processing was done using softwares IRAF, MIDAS and DAOPHOT-II. The values of the atmospheric extinction on the night of 2004 November 14/15 determined from the observations of PG 0231+051 bright stars are 0.53, 0.24, 0.14, 0.10 and 0.07 mag in U, B, V, R_c and I_c filters, respectively. The six standard stars in the PG 0231+051 field cover a range of $−0.329 < (B − V) < 1.448$

---

[1] http://asc.harvard.edu.

Table 1. The identification number, standard V, $(U − B)$, $(B − V)$, $(V − R)$ and $(R − I)$ photometric magnitudes of the secondary stars in the SN 2004et field are given. Uncertainties are indicated in the parenthesis.

ID	V (mag)	$U − B$ (mag)	$B − V$ (mag)	$V − R$ (mag)	$R − I$ (mag)
1	17.10 (0.012)	0.97 (0.114)	1.21 (0.021)	0.67 (0.022)	0.74 (0.032)
2	18.48 (0.015)	0.02 (0.108)	0.92 (0.031)	0.52 (0.020)	0.65 (0.055)
3	17.66 (0.013)	0.02 (0.038)	0.77 (0.022)	0.38 (0.045)	0.61 (0.059)
4	17.39 (0.011)	0.31 (0.035)	0.94 (0.019)	0.46 (0.013)	0.68 (0.029)
5	17.46 (0.013)	0.20 (0.045)	0.84 (0.022)	0.42 (0.014)	0.65 (0.030)
6	14.15 (0.009)	1.23 (0.013)	1.36 (0.012)	0.74 (0.010)	0.78 (0.023)
7	14.28 (0.009)	1.06 (0.012)	1.28 (0.012)	0.65 (0.010)	0.82 (0.023)
8	14.78 (0.009)	0.13 (0.010)	0.74 (0.013)	0.44 (0.010)	0.53 (0.023)
9	13.80 (0.009)	0.09 (0.010)	0.63 (0.012)	0.39 (0.010)	0.40 (0.023)
10	14.71 (0.009)	0.33 (0.010)	0.82 (0.012)	0.49 (0.010)	0.46 (0.023)
11	14.73 (0.010)	0.62 (0.012)	1.07 (0.013)	0.59 (0.011)	0.67 (0.023)

in colour and of $12.770 < V < 16.110$ in brightness. This gives the following transformation coefficients:

$$u_{ccd} = U − (0.061 ± 0.005)(U − B) + (6.937 ± 0.004),$$
$$b_{ccd} = B − (0.015 ± 0.004)(B − V) + (4.674 ± 0.004),$$
$$v_{ccd} = V − (0.011 ± 0.006)(B − V) + (4.223 ± 0.006),$$
$$r_{ccd} = R − (0.001 ± 0.011)(V − R) + (4.136 ± 0.007),$$
$$i_{ccd} = I − (0.023 ± 0.018)(R − I) + (4.619 ± 0.012),$$

where U, B, V, R, I are standard magnitudes and u_{ccd}, b_{ccd}, v_{ccd}, r_{ccd}, i_{ccd} represent the instrumental magnitudes normalized for 1 s of exposure and corrected for atmospheric extinction. The colour coefficients, zero-points and errors in them were determined by fitting least-squares linear regressions to the data points. Using the transformation coefficients obtained, *UBVRI* photometric magnitudes of 11 secondary stars were determined in the SN 2004et field and their average values are listed in Table 1 and marked in Fig. 1. The uncertainties are indicated in the parentheses.

Li et al. (2005) present the magnitudes of eight secondary standards in the field of SN 2004et. The zero-point differences, based on comparison of seven secondary standards in the field of SN 2004et, between our photometry and that of Li et al. (2005) are 0.033, −0.001 and 0.016 in B, V and R filters, respectively. This shows that our photometric calibration is secure. We cannot compare the U- and I-band magnitudes as Li et al. (2005) mention the U- and I-band magnitudes for only two secondary stars; differences are based on the comparison of the seven secondary stars in the field of SN 2004et.

Several short exposures, with exposure time varying from 60 to 1800 s, were taken to image SN 2004et. The data have been binned in $2 × 2$ pixel^2 because the data are oversampled and data analysis is simplified having a higher signal-to-noise ratio per pixel with fewer pixels. The SN was differentially calibrated with respect to the secondary stars 6, 7, 8 and 9 listed in Table 1. A full compilation of SN 2004et magnitudes in *UBVRI* filters derived in this way along with errors is presented in Table 2.

2.3 GMRT radio observations and data analysis

We observed SN 2004et with the Giant Metrewave Radio Telescope (GMRT) on 2005 January 02. GMRT is a synthesis array radio telescope consisting of 30 dish antennae of diameter 45 m each. The

observations in a frequency band centred at 1390 MHz, with a bandwidth of 16 MHz (divided into a total 128 frequency channels). The total no of antennae available for our observations were 27. The total time spent on the observation was 4 h, out of which we spent 2.5 h tracking the target source field of view (FoV). 3C48 was used as a flux calibrator. The flux density of 3C48 was derived using Baars formulation (Baars et al. 1977) extrapolated to the observed frequency. For phase calibration, we used the source from VLA catalogue 2022+616. Sources 3C48 and 2022+616 were also used for bandpass calibration. 3C48 was observed twice, for 10 min each once at the start of the observations and once towards the end. The phase calibrator was observed for 6 min after every 25 min observation of the SN FoV. Observation of the phase calibrator at small time intervals was important not only for tracking the instrumental phase and gain drifts, atmospheric and ionospheric gain and phase variations, but also for monitoring the quality and sensitivity of the data and for spotting occasional gain and phase jumps.

The data were analysed using Astronomical Image Processing System (AIPS) software developed by National Radio Astronomy Observatory (NRAO). One clean channel was picked up and VPLOT was used to look for dead antennae and obviously bad baselines. Bad antennae and corrupted data were removed using standard AIPS routines. Data were then calibrated and images of the fields were formed by Fourier inversion and CLEANing using AIPS task 'IMAGR'. For 1390-MHz observations, the bandwidth smearing effect was negligible and imaging was done after averaging 100 central frequency channels. The whole field was divided into two subfields to take care of the wide field imaging. We performed a few rounds of phase self-calibration to remove the phase variations due to the bad weather and related causes and improved the images a good deal.

The flux density of 3C48 using Baars formulation is 16.15 Jy. The flux density of the phase calibrator was $1.82 ± 0.07$ Jy. AIPS task 'JMFIT' was used to fit the Gaussian at the SN position and obtain the flux density. The flux density of SN 2004et was found to be $1.24 ± 0.24$ mJy. The map rms of the SN FoV was 90 μJy and the map resolution was $3.20 × 2.40$ arcsec^2. The J2000 position of the SN 2004et obtained from our GMRT observations in RA and Dec. was $20^h 35^m 25^s.40 ± 0^s.02$ and $60°07'17''.90 ± 0''.12$, respectively, consistent with the optical position of the SN. Fig. 2 shows the radio contour map of SN 2004et FoV.

3 X-RAY ANALYSIS

3.1 X-ray spectra

We extracted counts and spectra in the 0.5–8 keV bandpass from the location of the SN using ACIS Extract version 3.107 (Broos et al. 2002). The source extraction region was chosen to enclose 90 per cent of the point spread function at 1.5 keV, which resulted in a roughly circular region of ∼1 arcsec radius. We obtained 204, 153 and 156 counts for the three observations. Our background region was a source-free annulus centred on the SN with an inner radius of 6 arcsec and an outer radius of 27 arcmin. This background region contained ∼100 counts in each observation; we therefore expect the source extraction region to contain 0.14 background counts on average. Response files were made using ACIS Extract, which calls the CIAO tools mkacisrmf and mkarf.

We grouped the spectra to contain at least 15 counts/bin and fit them in Sherpa (Freeman, Doe & Siemiginowska 2001) using standard χ^2 statistics. We fit two simple models: an absorbed power law and an absorbed mekal plasma with elemental abundances allowed to vary. In the mekal fits, if an elemental abundance was

Table 2. *UBVR*$_c$ and *I*$_c$ magnitudes of SN 2004et along with errors, Julian Date and mid-UT of observations are listed.

Date (UT)	Time (JD)	U (mag)	B (mag)	V (mag)	R$_c$ (mag)	I$_c$ (mag)
2004 10 06.630	245 3285.1296	12.44 ± 0.016	12.95 ± 0.014	12.60 ± 0.019	12.27 ± 0.013	11.94 ± 0.019
2004 10 13.616	245 3292.1162		12.88 ± 0.032	12.50 ± 0.027	12.16 ± 0.027	11.88 ± 0.029
2004 10 15.584	245 3294.0844		13.20 ± 0.010	12.62 ± 0.014	12.22 ± 0.016	11.91 ± 0.015
2004 10 16.603	245 3295.1031	13.15 ± 0.011	13.21 ± 0.013	12.62 ± 0.013	12.23 ± 0.020	11.88 ± 0.015
2004 10 17.552	245 3296.0517	13.26 ± 0.018	13.26 ± 0.010	12.63 ± 0.026	12.24 ± 0.021	11.87 ± 0.031
2004 10 18.573	245 3297.0726	13.40 ± 0.013	13.31 ± 0.013	12.66 ± 0.021	12.23 ± 0.030	11.88 ± 0.024
2004 10 19.607	245 3298.1072	13.50 ± 0.023	13.37 ± 0.016	12.63 ± 0.019	12.21 ± 0.036	11.89 ± 0.031
2004 10 20.568	245 3299.0677	13.63 ± 0.010	13.41 ± 0.013		12.23 ± 0.019	11.90 ± 0.018
2004 10 21.554	245 3300.0543	13.72 ± 0.012	13.47 ± 0.009	12.67 ± 0.014	12.22 ± 0.018	11.88 ± 0.020
2004 10 22.560	245 3301.0596	13.81 ± 0.012	13.52 ± 0.006	12.69 ± 0.016	12.25 ± 0.014	11.89 ± 0.017
2004 11 03.570	245 3313.0698	14.77 ± 0.007	13.96 ± 0.003	12.84 ± 0.004	12.33 ± 0.006	11.91 ± 0.008
2004 11 04.542	245 3314.0422	14.83 ± 0.007	13.99 ± 0.008	12.85 ± 0.008	12.32 ± 0.009	11.92 ± 0.008
2004 11 05.570	245 3315.0699	14.89 ± 0.006	14.02 ± 0.006	12.87 ± 0.007	12.33 ± 0.010	11.90 ± 0.014
2004 11 06.548	245 3316.0476	14.95 ± 0.010	14.04 ± 0.007	12.87 ± 0.010	12.34 ± 0.010	11.90 ± 0.013
2004 11 08.550	245 3318.0504	15.06 ± 0.005	14.08 ± 0.004	12.89 ± 0.006	12.35 ± 0.009	11.90 ± 0.008
2004 11 13.550	245 3323.0499	15.32 ± 0.038	14.23 ± 0.011	12.93 ± 0.005	12.35 ± 0.014	11.90 ± 0.012
2004 11 14.543	245 3324.0431	15.37 ± 0.010	14.21 ± 0.003	12.93 ± 0.010	12.35 ± 0.008	11.90 ± 0.009
2004 11 16.538	245 3326.0377	15.48 ± 0.011	14.24 ± 0.003	12.94 ± 0.004	12.36 ± 0.008	11.89 ± 0.012
2004 11 18.541	245 3328.0415	15.62 ± 0.012	14.31 ± 0.007	12.97 ± 0.013	12.37 ± 0.012	11.92 ± 0.010
2004 12 02.572	245 3342.0717	16.18 ± 0.018	14.52 ± 0.004	13.04 ± 0.003	12.40 ± 0.004	11.91 ± 0.010
2004 12 03.587	245 3343.0867	16.16 ± 0.015	14.54 ± 0.004	13.05 ± 0.003	12.41 ± 0.005	11.92 ± 0.005
2004 12 04.574	245 3344.0742	16.22 ± 0.013	14.56 ± 0.011	13.06 ± 0.016		11.92 ± 0.030
2004 12 12.539	245 3352.0389	16.54 ± 0.017	14.69 ± 0.004	13.11 ± 0.007	12.44 ± 0.007	11.92 ± 0.010
2004 12 13.535	245 3353.0353		14.71 ± 0.005	13.14 ± 0.003	12.48 ± 0.004	
2004 12 15.578	245 3355.0783		14.73 ± 0.002	13.15 ± 0.001	12.47 ± 0.002	11.96 ± 0.002
2004 12 16.551	245 3356.0512	16.63 ± 0.031	14.76 ± 0.003	13.15 ± 0.002	12.48 ± 0.004	11.93 ± 0.008
2004 12 18.560	245 3358.0597		14.80 ± 0.003	13.18 ± 0.002	12.49 ± 0.003	11.98 ± 0.003
2004 12 22.546	245 3362.0456				12.50 ± 0.012	11.99 ± 0.009
2005 01 02.560	245 3371.0601					12.10 ± 0.006
2005 10 13.615	245 3657.1147		19.15 ± 0.047	18.32 ± 0.020	17.31 ± 0.018	16.84 ± 0.018
2005 10 14.615	245 3658.1147		19.15 ± 0.047	18.31 ± 0.020	17.31 ± 0.018	16.84 ± 0.017
2005 10 27.560	245 3671.0601		19.43 ± 0.038	18.41 ± 0.018	17.50 ± 0.014	
2005 10 29.576	245 3673.0760		19.45 ± 0.028	18.51 ± 0.017	17.59 ± 0.017	
2005 11 02.598	245 3677.0980		19.48 ± 0.019	18.54 ± 0.020	17.59 ± 0.015	
2005 11 04.544	245 3679.0438		19.53 ± 0.031	18.55 ± 0.014	17.61 ± 0.024	17.15 ± 0.019
2005 11 05.557	245 3680.0571	20.26 ± 0.069	19.49 ± 0.022	18.59 ± 0.015	17.65 ± 0.015	17.16 ± 0.020
2005 11 06.577	245 3681.0770	20.27 ± 0.081	19.53 ± 0.018	18.61 ± 0.017	17.70 ± 0.014	17.23 ± 0.017
2005 11 07.558	245 3682.0576		19.54 ± 0.026	18.61 ± 0.017	17.67 ± 0.016	17.21 ± 0.016
2005 11 09.530	245 3684.0298			18.70 ± 0.026	17.74 ± 0.019	17.20 ± 0.037
2005 11 22.561	245 3697.0610		19.60 ± 0.037	18.78 ± 0.021	17.91 ± 0.018	
2005 11 23.560	245 3698.0598		19.62 ± 0.039	18.79 ± 0.024	17.92 ± 0.015	
2005 11 24.551	245 3699.0512		19.66 ± 0.033	18.83 ± 0.020	17.96 ± 0.019	
2005 12 03.600	245 3708.1001			18.94 ± 0.026	18.07 ± 0.020	17.54 ± 0.031
2005 12 05.570	245 3710.0699	20.41 ± 0.067	19.80 ± 0.030	18.99 ± 0.013	18.12 ± 0.014	17.66 ± 0.015
2005 12 06.545	245 3711.0447		19.79 ± 0.023	18.90 ± 0.025	18.16 ± 0.022	17.64 ± 0.036
2005 12 08.577	245 3713.0766	20.66 ± 0.244	19.83 ± 0.040	19.04 ± 0.022	18.15 ± 0.021	17.64 ± 0.026
2005 12 09.556	245 3714.0565		19.85 ± 0.044	19.03 ± 0.029	18.11 ± 0.020	17.68 ± 0.026
2005 12 18.553	245 3723.0534			19.11 ± 0.023	18.29 ± 0.014	
2005 12 19.554	245 3724.0538			19.11 ± 0.038		
2005 12 20.567	245 3725.0674			19.01 ± 0.024	18.23 ± 0.022	17.73 ± 0.047
2005 12 21.550	245 3726.0502			19.14 ± 0.042	18.33 ± 0.019	17.86 ± 0.051
2006 01 04.552	245 3738.0524			19.38 ± 0.037	18.59 ± 0.024	
2006 01 05.556	245 3739.0561		20.22 ± 0.099	19.35 ± 0.037	18.58 ± 0.036	

consistent with solar, i.e. its 1σ confidence interval included the solar value, we froze that abundance and refit in order to find any potential non-solar abundances. In all cases (power law and mekal), the absorbing column was consistent with the value of $n_H = 2.3 \times 10^{21}$ cm^{-2} inferred from the measurement of $E(B - V) = 0.41$ mag (Zwitter et al. 2004), using the conversion of 5.55 ×

10^{21} cm^{-2} mag^{-1} (Predehl & Schmitt 1995). We therefore froze the column density at this value and refit the spectra. The results can be found in Table 3. We also give the unabsorbed flux over the *Chandra* bandpass; the uncertainty in this flux estimate is derived from the uncertainty in the model normalization, found via the projection command in Sherpa.
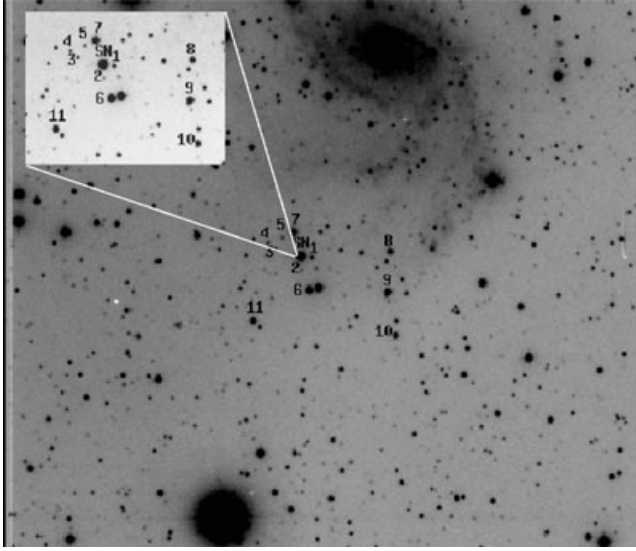
Figure 1. SN 2004et field observed with the 1.04-m ST at ARIES, Nainital. Inset shows the location of SN and marked are the comparison stars.
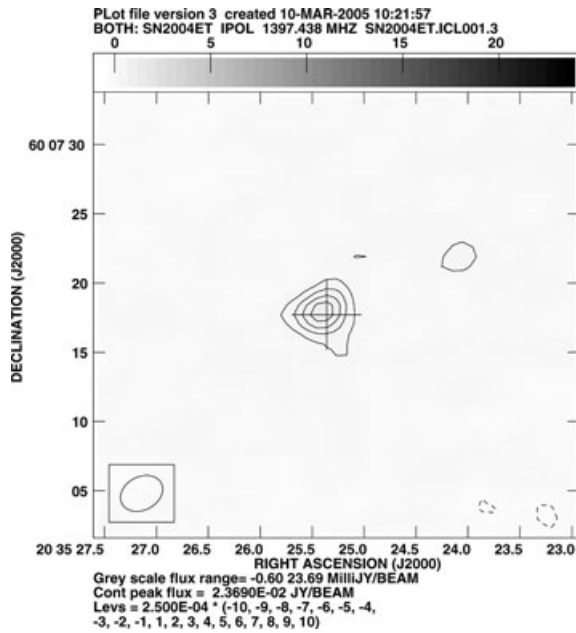

Figure 2. Radio contour map of SN 2004et obtained with the GMRT on 2005 January 02. The cross shows the optical position of the SN 2004et.

Although these models may be too simplistic, they both show that the X-ray spectrum softens with time, and they are both in fairly good agreement on the unabsorbed flux. Given the low statistical quality of the spectra, more complex models are not warranted. We note that, although the data do not have much power to distinguish different spectral models, both the power-law model and the Mekal model with solar abundances provide statistically unacceptable fits to the second observation (without letting the abundances vary, the Mekal fit had a χ^2/d.o.f. $= 17.4/8$). The discrepancy between the data and these models could be due to emission from O, Fe, Si and Ca near 0.7, 1.1, 2.1 and 3.8 keV, respectively, as indicated by the mekal spectra fits with these abundances allowed to vary (see Fig. 3). However, this is not conclusive. The best-fitting abundances are O $= 56^{+35}_{-23}$, Si $= 25^{+20}_{-16}$, Ca $= 275^{+112}_{-109}$ and Fe $= 11^{+7}_{-4}$, all values with respect to solar.

(Rho et al. 2007) reported that the first observation is best fitted by a 'thermal model' with a temperature of $kT = 1.3$ keV and a lower limit of 0.5 keV. They also report a significantly enhanced column of $n_H = 1 \times 10^{22}$ cm^{-2}. However, our Mekal model prefers a much higher temperature for the first observation, $kT = 20$ keV, with a lower limit of 14 keV, and the index of our power-law model also suggests a harder spectrum than a 1.3-keV plasma would be expected to produce. We are unable to reproduce the low temperature found by Rho et al. (2007), with either the Mekal model or Raymond–Smith or thermal bremsstrahlung models. An absorbed Raymond–Smith model (with the column density allowed to vary) gives a temperature of $kT = 22^{+42}_{-13}$ keV (with $n_H = 2.3^{+0.6}_{-0.5} \times 10^{21}$ cm^{-2}). An absorbed bremsstrahlung model gives a temperature of $kT = 14^{+\infty}_{-4}$ keV (with $n_H = 2.5^{+0.6}_{-0.5} \times 10^{21}$ cm^{-2}). The reason for this discrepancy between our results and those of Rho et al. (2007) are unclear, but their thermal model may have a fairly different distribution of flux than the ones tried here.

3.2 X-ray evolution

We characterize the X-ray luminosity evolution as a power law in time, $L_X \propto t^{-\alpha}$. We use the average of the fluxes from both models as the best estimate of the flux from each observation. Using a distance of 5.5 Mpc, the X-ray luminosities are $(3.0 \pm 0.3) \times 10^{38}$, $(2.3 \pm 0.3) \times 10^{38}$ and $(2.1 \pm 0.2) \times 10^{38}$ erg s^{-1}. The best-fitting α is 0.4 ± 0.2. The X-ray light curve is plotted in Fig. 4. The spectral evolution can be seen by separately plotting the soft band (0.5–2 keV) and hard band (2–8 keV) fluxes (Fig. 4). The soft X-ray luminosity is nearly constant, while the hard band decays with a power-law index of $\alpha_{hard} = 0.8 \pm 0.2$. This is very different than the evolution of the type IIP 1999em observed by *Chandra* (Pooley et al. 2002); in that case, both the hard and soft bands were seen to decay.

We further explore the spectral evolution by examining the temperature evolution, as estimated by the single-temperature Mekal models (Table 3). We plot the X-ray temperature as a function of

Table 3. *Chandra* observation details and spectral fit parameters for either a power-law model or mekal plasma model.

ObsID	Date (UT)	Exposure time (s)	T (d)	PL index	F_X (0.5–8 keV) (erg cm^{-2} s^{-1})	χ^2/d.o.f.	Mekal kT (keV)	F_X [0.5–8 keV] (erg cm^{-2} s^{-1})	χ^2/d.o.f.	Non-solar abundance
4631	2004 October 22.2	29 740.2	30.2	$1.3^{+0.1}_{-0.1}$	$8.3^{+0.9}_{-0.9} \times 10^{-14}$	11.5/12	20^{+11}_{-6}	$8.2^{+0.6}_{-0.6} \times 10^{-14}$	11.9/12	–
4632	2004 November 06.0	27 980.4	45.0	$1.6^{+0.2}_{-0.2}$	$5.8^{+0.7}_{-0.7} \times 10^{-14}$	17.2/8	$3.9^{+1.0}_{-0.8}$	$6.4^{+1.0}_{-1.0} \times 10^{-14}$	4.5/4	O, Si, Ca, Fe
4633	2004 December 03.5	26 615.5	72.5	$1.9^{+0.2}_{-0.2}$	$5.9^{+0.6}_{-0.6} \times 10^{-14}$	5.9/9	$2.8^{+0.7}_{-0.4}$	$5.5^{+0.7}_{-0.7} \times 10^{-14}$	2.2/8	Ca

Notes: T = time since explosion, taken to be 2004 September 22.0 (Li et al. 2005); PL = power law; all fluxes are unabsorbed; confidence intervals are 1σ.
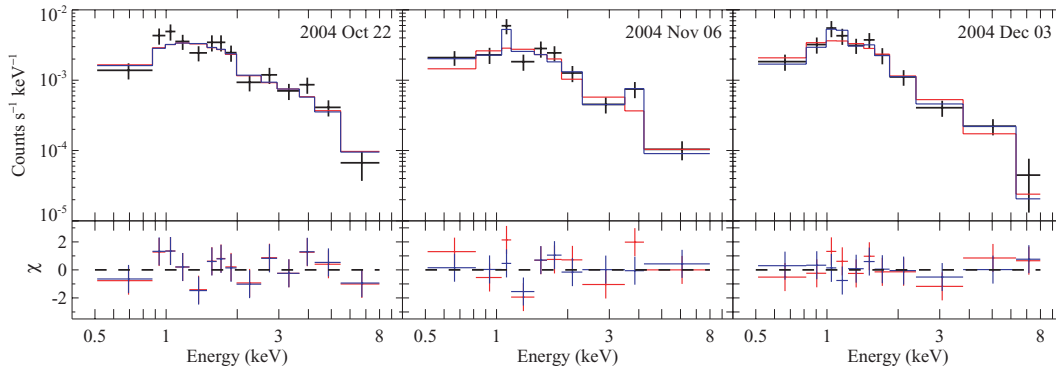
Figure 3. *Chandra* spectra of SN 2004et with power-law fits (red) and mekal plasma fits (blue). The residuals are plotted in the bottom panels as (data − model)/error with vertical bars of length ±1.
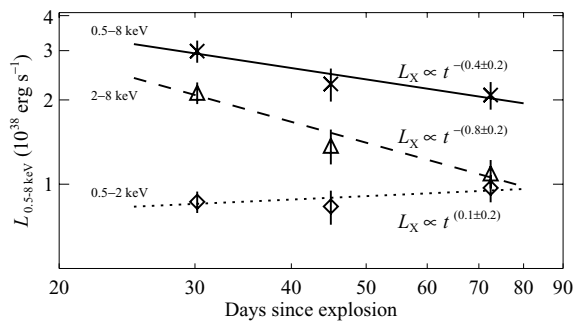

Figure 4. *Chandra* light curves of SN 2004et with power-law fits. The solid line is the best-fitting power law for the full 0.5–8 keV luminosities (represented by ×). The dashed line is for the hard band (2–8 keV) luminosities (represented by triangles). The dotted line is for the soft band (0.5–2 keV) luminosities (represented by diamonds).
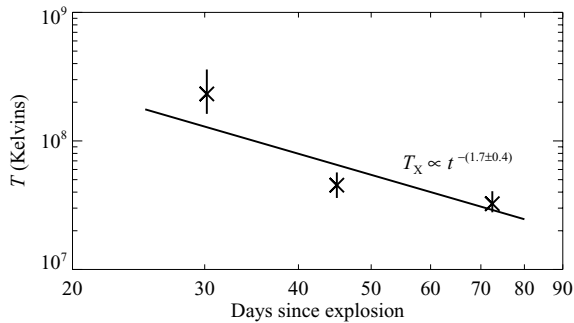
Figure 5. X-ray temperature evolution of SN 2004et with power-law fit.

time in Fig. 5. The evolution can be roughly characterized as a power law in time, $T_X \propto t^{-\beta}$, with a best-fitting $\beta = 1.7 \pm 0.4$.

4 PHOTOMETRIC EVOLUTION

In this section we present the results of our photometric observations. Since this SN is located 247.1 arcsec east and 115.4 arcsec south of the nucleus of NGC 6946, the contribution from the galaxy is negligible in determining the SN magnitudes.

4.1 Reddening towards SN 2004et

The high-resolution spectra obtained by Zwitter et al. (2004) shows a relatively featureless spectrum with very broad, low-

contrast Hα emission but the presence of sharp interstellar Na I absorption lines. The equivalent width of Na I D II lines corresponds to an estimated total reddening of $E(B - V) = 0.41$ mag. The Galactic extinction towards SN 2004et is $E(B - V) = 0.34$ mag using the reddening maps of Schlegel et al. (1998) which corresponds to $A_V^{gal} = 1.06$ mag for a $R_V = 3.1$. But the total extinction is $E(B - V) = 0.41$ mag, thus the rest of it may be attributed due to the host galaxy. Li et al. (2005) adopt a total reddening of $E(B - V) = 0.41 \pm 0.07$ mag towards SN 2004et. The lower limit of this corresponds to no reddening due to the host galaxy. We adopt a total reddening (galactic + host) of $E(B - V) = 0.41 \pm 0.07$ mag for our further analysis.

4.2 Light curves

The $UBVR_cI_c$ photometric data obtained from ∼14 d to ∼470 d since explosion at 53 epochs is compiled in Table 2. We do not have observations near the explosion epoch which are very important to study the overall temporal evolution of the light curve. For this purpose, we have combined the early-time data points reported by Li et al. (2005) and the pre-discovery magnitudes by Klotz, Pollas & Boer (2004) and collaborators Itagaki & Yamaoka (2004). A few *V*-band data points by Lindberg (2004) are included at the transition from plateau to tail. The data set by Li et al. (2005) matches best with ours as the comparison stars for the two data sets are similar, as mentioned in Section 2. This allows us to cross-compare our photometry with other data available in the literature. *U*-band observations, though small in number, were obtained whenever possible since they are valuable to construct the bolometric light curve especially at early times. The combined $UBVR_cI_c$ light curve is shown in Fig. 6, and is typical of SNe II plateau. Fig. 6 also shows the light curves of SN 1999em and SN 1999gi shifted arbitrarily to match those of the SN 2004et light curves. There is a rapid decline in the *U* band which is followed by a slow decline of the *B* band during the first 100 d after the explosion. The decline in the *B* band during the first 100 d as estimated by Sahu et al. (2006) is $\beta_{100}^B = 2.2$ mag. Patat et al. (1994) classified SNe II as plateau and linear on the basis of the *B*-band decline rates. SNe IIP have $\beta_{100}^B < 3.5$ compared to type IIL which have $\beta_{100}^B > 3.5$. The obtained value of β_{100}^B for SN 2004et establishes it as an SN IIP at least according to Patat's classification scheme.

The light curve clearly shows a pronounced plateau of constant luminosity in the V, R_c, I_c bands. The plateau length is estimated to be about 110 ± 10 d from the *V*-band light curve. SNe IIP after
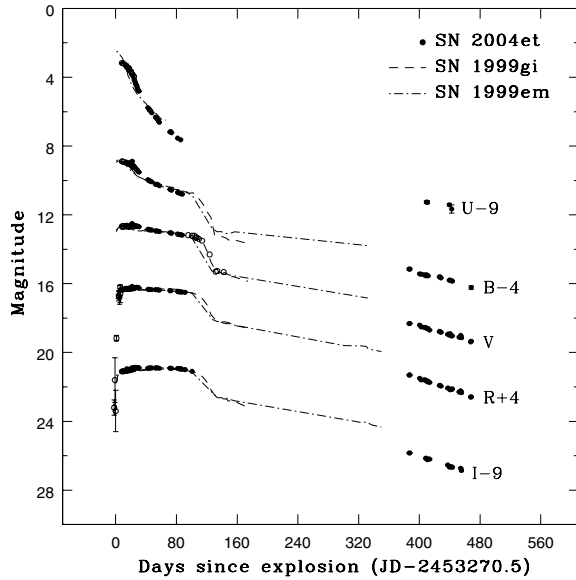
Figure 6. $UBVR_cI_c$ light curve of SN 2004et (filled circle: our data), including those available in the literature (open circle): the early data points by Li et al. (2005), the pre-discovery magnitudes by Klotz et al. (2004) and V-band magnitude from Lindberg (2004). The light curves have been shifted by arbitrary amount as indicated in the figure. Also the light curves of SN 1999em ($UBVRI$: dash–dotted line) and SN 1999gi ($BVRI$: dashed line) have been included for comparison and shifted arbitrarily in order to match the corresponding light curves of SN 2004et.

the explosion, start cooling slowly to the recombination temperature of hydrogen and radiate energy deposited into hydrogen from the initial shock. This recombination gives rise to a pronounced plateau in the light curve during which the expansion and cooling of the photosphere balance each other so that the luminosity remains almost constant. Immediately after the plateau phase, we note a steep decline in the V-band light where the magnitude falls from 13.50 at 113 d to 15.32 at 142 d after the explosion. This fall of $\sim$2 mag in $\sim$30 d is clearly seen in the V-band light curve. There is a drop in the observed flux in all other passbands after the plateau phase. This fall indicates that the hydrogen recombination wave has receded completely through the massive hydrogen envelope and the SN now enters the nebular phase. We lack the early nebular phase observations. The decline rates stated by Sahu et al. (2006) from $\sim$180 to $\sim$310 d after the explosion in the early nebular phase in B, V, R and I bands are 0.64, 1.04, 1.01 and 1.07 mag, respectively. The flux variation in this phase is marked by the radioactive decay of ^{56}Co to ^{56}Fe with an expected decay rate of 0.98 mag/100 d particularly in the V band (Patat et al. 1994). Except for the B band, the decline rates during the early nebular phase in V, R and I bands agree fairly well with the expected decay rate of ^{56}Co to ^{56}Fe, suggesting that little or no γ-rays escaped during this time. Fig. 7 shows the later nebular phase of the light curve from 386 to 469 d since explosion with the slope of 1.24 mag/(100 d) in the V band. Post 370 d the decline rate during the later nebular phase in BVR_cI_c bands is 1.01, 1.24, 1.47 and 1.49 mag/(100 d). The decay rate beyond $\sim$370 d are quite steep as compared to those in the early nebular phase. The decay rate in the nebular phase deviates from the ^{56}Co to ^{56}Fe decay implying the leakage of γ-rays and the SN becoming transparent to the γ-rays or dust formation in the SN ejecta. Sahu et al. (2006) suggest dust formation in the SN ejecta around $\sim$320 d.
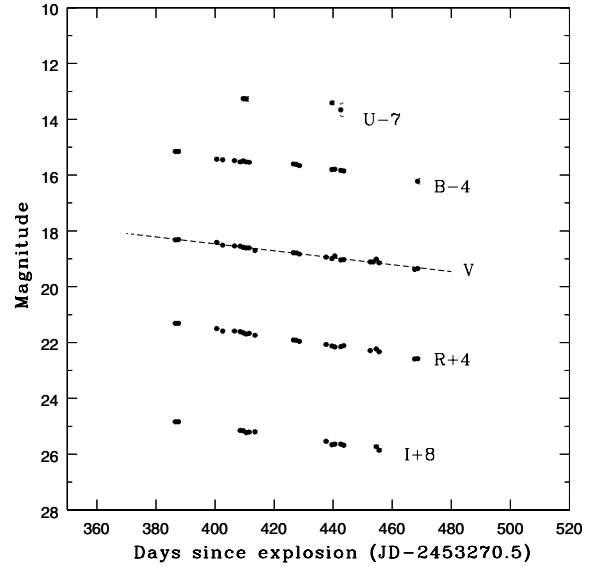

Figure 7. $UBVR_cI_c$ light curve of SN 2004et during the late tail phase. The dashed line indicates the slope of 1.24 mag/(100 d) in the V band which is steeper than the expected decay of 0.98 mag/(100 d) for ^{56}Co to ^{56}Fe decay. The light curves have been shifted by arbitrary amount as indicated in the figure.
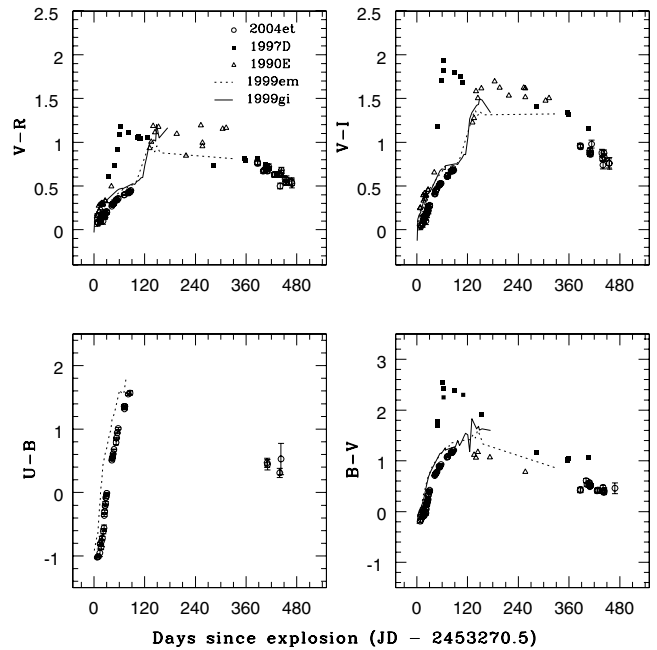

Figure 8. Colour evolution of SN 2004et (unfilled circle) compared with that of SN 1999em (dotted line), SN 1999gi (solid line), SN 1997D (filled squares) and SN 1990E (unfilled triangles) corrected for a reddening of $E(B - V) = 0.41$, 0.06, 0.21, 0.02 and 0.48, respectively.

4.3 Colour evolution

In Fig. 8 we show the colour evolution of SN 2004et along with that of SN 1999em, SN 1999gi, SN 1997D and SN 1990E for comparison. The explosion epochs for these SNe are well established and taken to be JD 245 1475.6 (Leonard et al. 2002a), JD 245 1526.2 (Leonard et al. 2002b), JD 245 0430.0 (Benetti et al. 2001) and JD 244 7932.0 (Schmidt et al. 1993) for SN 1999em, SN 1999gi, SN

1997D and SN 1990E, respectively. The colours of these SNe were corrected for a total reddening (galactic + host) adopting the following $E(B - V)$ values of 0.41, 0.06, 0.21, 0.02 and 0.48 for SN 2004et, SN 1999em, SN 1999gi, SN 1997D and SN 1990E, respectively. The $U - B$ and $B - V$ colour evolution of SN 2004et is slower than that of SN 1999em which has also been studied by Li et al. (2005) during the first month of evolution. For comparison we show the colour evolution of the prototypical faint SN 1997D. At the end of the plateau phase the colours of SN 1997D show a sharp rise and an excess in colour as compared to other SNe. This has been recognized to be a characteristic of faint low-luminosity SNe such as SN 1997D, SN 1999eu (Pastorello et al. 2004). Colour evolution of SN 1990E is also quite rapid but it does not reach a significant excess except in $V - I$ colour. Till $\sim$100 d after the explosion the overall colours of SN 2004et are bluer as compared to other SNe. Lack of observations at the transition from plateau to tail phase restricts us to comment on the colour evolution. Sahu et al. (2006) mention that the $(B - V$ and $V - R)$ colours of SN 2004et are similar to other SN IIP whereas the $(R - I)$ colour of SN 2004et is still bluer as compared to SN 1999em beyond $\sim$200 d. No unusual change in colour is noticed around the dust-formation time.

4.4 Temporal evolution of photospheric radius and colour temperature during the plateau phase

The temporal evolution of radius and colour temperature is studied during the plateau phase of SN 2004et by the Expanding Photosphere Method (EPM) summarized by Hamuy et al. (2001). The methodology in brief is discussed in this section. Hamuy et al. (2001) assume that if the continuum radiation arises from a spherically symmetric photosphere, the photometric colour and magnitude determines the angular radius of photosphere given by

$$\theta = \frac{R}{D} = \sqrt{\frac{f_\lambda}{\zeta_\lambda^2 B_\lambda(T) 10^{-0.4A(\lambda)}}}, \tag{1}$$

where R is the photospheric radius, D is the distance to the SN, $B_\lambda(T)$ is the Planck function at the colour temperature of the blackbody radiation, f_λ is the apparent flux density and $A(\lambda)$ is the extinction. Here ζ_λ accounts for the fact that a real SN does not radiate like a blackbody at a unique colour temperature. The implementation of this requires one to make blackbody fits to the observed magnitudes. This involves the determination of synthetic broad-band magnitudes from Planck spectra. Hamuy et al. (2001), now compute $b_{\bar\lambda}(T)$, the magnitude of $\pi B_{\bar\lambda}(T)$ for a filter with central wavelength $\bar\lambda$, to which the following polynomial is fitted in the temperature range of 4000–25 000 K:

$$b_{\bar\lambda}(T) = \sum_{i=1}^{5} C_i(\lambda) \left(\frac{10^4 K}{T} \right)^i. \tag{2}$$

The values of the coefficients $C_i(\lambda)$ are listed in table 13 of Hamuy et al. (2001). The colour temperature are now computed at each epoch using these fits for any combination of magnitude by a χ^2 minimization technique. The dilution factor (ζ_S) is calculated for our photometric system by performing polynomial fits to $\zeta_S(T_S)$ given by Hamuy et al. (2001) mentioned below:

$$\zeta_S(T_S) = \sum_{i=0}^{2} a_{S,i} \left(\frac{10^4 K}{T_S} \right)^i, \tag{3}$$

where S is the filter combination used to fit the atmosphere models with blackbody curves. The coefficients $a_{S,i}$ for different filter
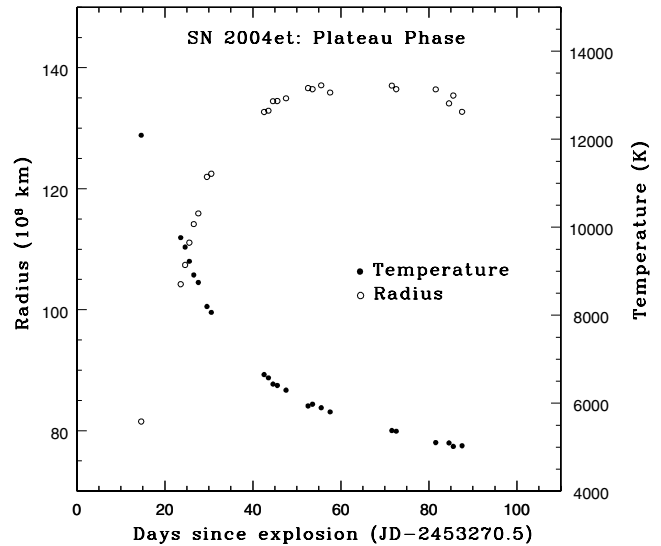

Figure 9. Temporal evolution of the photospheric radius at the thermalization depth and the colour temperature for SN 2004et during the plateau phase.

combinations are listed in table 14 of Hamuy et al. (2001). Once the colour temperature and the values of ζ_λ for different filter combinations are calculated, the photospheric radius at each epoch can be obtained using equation (1) for a known SN distance D.

Adopting the above approach by Hamuy et al. (2001) we compute the colour temperature using *BVRI* filters and the corresponding photospheric radius for the plateau phase of SN 2004et using A_V^{tot} (galactic + host) = 1.27. The temporal evolution of colour temperature and radius is shown in Fig. 9. We find that the initial colour temperature was $\sim$12 100 K and the SN cooled to $\sim$5000 K till $\sim$90 d after the explosion. While the photosphere was cooling during the first 90 d in the plateau phase, the photospheric radius was increasing due to the constant expansion of the ejecta. It is this balance between the steady increase in radius and the decrease in temperature which very well explains the constant luminosity plateau seen in SN IIP light curves.

4.5 The bolometric light curve

The integrated flux in $UVOI_cR_c$ bands gives a meaningful estimate of the bolometric luminosity. The bolometric luminosity in the tail phase provides an accurate estimate of the ^{56}Ni mass ejected in the explosion. The distance to the host galaxy NGC 6946 is well estimated using different methods such as the H I Tully–Fisher relation (Pierce 1994), the CO Tully–Fisher relation (Schoniger & Sofue 1994) and the EPM for type II SNe (Schmidt et al. 1994). We adopt a mean distance of 5.5 ± 1.0 Mpc. To construct the bolometric light curve, we consider here the epochs which have observations in all $UBVR_cI_c$ bands. Our data set is supplemented by the early-time $UBVR_cI_c$ data by Li et al. (2005). The $UVOIR$ bolometric light curve is thus constructed using the dereddened magnitudes and the known distance to NGC 6946. The correction for the missing infrared (IR) flux has been applied by comparing with the bolometric light curve for SN 1987A. The redshift of the host galaxy NGC 6946 is very small ($z = 0.000\,16$; from NSASA/IPAC Extragalactic Database), we have therefore neglected the k-correction. The obtained magnitudes were converted to flux using calibrations by Bessell, Castelli & Plez (1998). The bolometric light curve of SN 2004et is shown
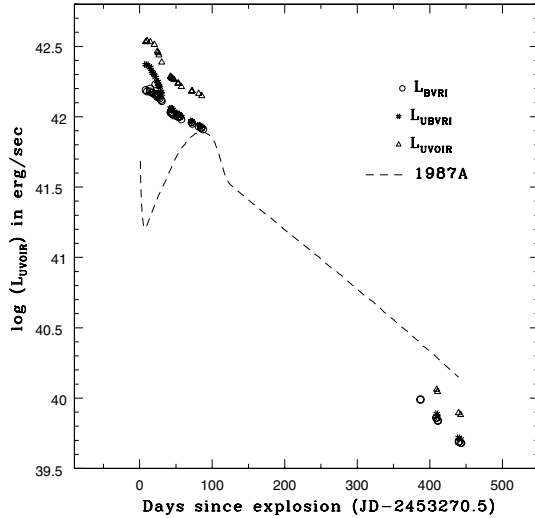
Figure 10. Bolometric light curve of SN 2004et after correcting for the contribution from near-IR bands (open triangles). For comparison we show the bolometric light curve constructed using $UBVR_cI_c$ bands (asterisks) and that from BVR_cI_c bands (open circles) to look for the contribution of U-band flux. The dashed line indicates the bolometric light curve of SN 1987A (Suntzeff & Bouchet 1990).

in Fig. 10. The U-band contribution at $\sim$8 d is $\sim$35 per cent and that from the I_c band is $\sim$11 per cent. The contribution from the U band decreases towards the end of the plateau phase whereas that from the I band increases. The similar trend is there for SN 1987A. In Fig. 11 we show the percentage contribution of flux in different bands of SN 2004et during the plateau and the late nebular phases. For a comparison, percentage contribution of flux in the case of SN 1987A in different bands has also been shown. We note that during the late nebular phase the contribution from the U band starts to increase and is $\sim$5 per cent and that from I_c band decreases and reached $\sim$28 per cent at $\sim$476 d. The U-band contribution during the initial days is significant as compared to I_c and R_c bands. We have taken into account any contribution from the near-IR bands while constructing the $UVOIR$ bolometric light curve. In Fig. 10 we show the $UVOIR$ bolometric light curve constructed from $UBVR_cI_c$ bands as asterisks. The open circles in the figure shows the contribution from the BVR_cI_c bands alone, showing that the U-band flux is dominant during the early phase. The open triangles show the $UVOI_cR_c$ bolometric light curve. The figure clearly shows that we miss out quite a lot of flux if we do not account for the contribution from the near-IR bands. The bolometric luminosity of the exponential tail gives an estimate of ^{56}Ni mass ejected during the explosion by a direct comparison to the bolometric light curve of SN 1987A (shown by dashed line in Fig. 10). The estimation of ^{56}Ni mass using the bolometric light curve is discussed in detail in the next section.

4.6 Physical parameters

4.6.1 Estimate of ejected nickel mass

The tail phase of the light curve of an SN IIP is thought to be powered by the radioactive decay of ^{56}Co to ^{56}Fe. The luminosity in the tail phase is directly proportional to the amount of nickel produced in the explosion. To estimate the amount of nickel produced in the explosion of SN 2004et, we use here different methods. These methods are briefly described below.
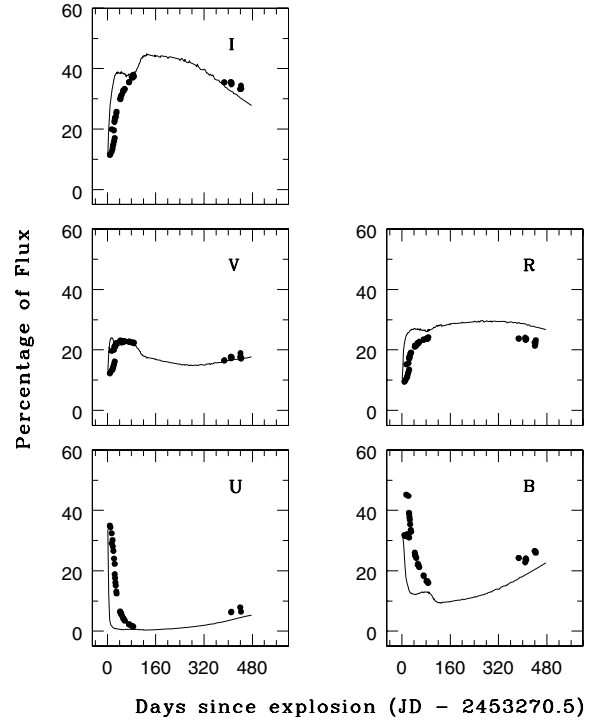

Figure 11. Flux contribution, in percentage, in $UBVR_cI_c$ bands of SN 2004et along with a comparison to SN 1987A.

(i) *Nickel mass from the bolometric luminosity of the exponential tail:* The nickel mass derived from the bolometric luminosity of the exponential tail as described by Hamuy (2003) assumes that all the γ-rays during the radioactive decay of ^{56}Co to ^{56}Fe are fully thermalized. It is to be noted here that ^{56}Co is the daughter nucleus of ^{56}Ni, thus the bolometric luminosity in the exponential tail is proportional to the ejected ^{56}Ni mass. The late-time decline rates for SN IIP are consistent with the decay of ^{56}Co to ^{56}Fe. The V band (V_t) magnitude in the exponential tail is first converted into bolometric luminosity (L_t) in erg s^{-1} using a total extinction of $A_V = 1.27$, a distance of 5.5 ± 1.0 Mpc and applying a bolometric correction of BC $= 0.26 \pm 0.06$. The nickel mass is then estimated by using equation (2) of Hamuy (2003). We estimate the nickel mass using this method at two different points in the tail and obtain an average value of nickel ejected in the explosion as $M_{Ni} = 0.06 \pm 0.03 \, M_{\odot}$.

(ii) *Nickel mass from 'steepness of decline' S correlation:* Elmhamdi, Chugai & Danziger (2003) present a correlation between the rate of decline from plateau to tail in the V band and the nickel mass. Elmhamdi et al. (2003) define a steepness 'S' parameter, which is the maximum gradient during transition in mag d^{-1}. Elmhamdi et al. (2003) using a sample of SN IIP conclude that the steepness 'S' anticorrelates with the ^{56}Ni mass. The smaller the amount of ^{56}Ni, the steeper will be the transition from the plateau to tail. For SN 2004et, we do not have a well-sampled V-band light curve during the transition from the plateau to the tail. Hence the determination of S will result in large uncertainties. Using the available data set we obtain $S = 0.07 \pm 0.02$ which results in $M_{Ni} = 0.056 \pm 0.016 \, M_{\odot}$ using equation (3) of Elmhamdi et al. (2003).

Sahu et al. (2006) also estimate the nickel mass by comparing the tail phase bolometric luminosity with that of SN 1987A during $\sim$250 to 300 d if we assume that the γ-ray deposition for both SN 2004et and SN 1987A is the same. The estimated mass of ^{56}Ni is

$0.048 \pm 0.01\,M_\odot$ for a value of $0.075\,M_\odot$ for SN 1987A (Turatto et al. 1998). But we lack the early nebular phase observations and towards the late nebular phase the γ-ray deposition for SN 2004et and SN 1987A is not really the same and there is evidence of dust formation around 310 d. Thus, we do not adopt this method for nickel mass estimation.

We discussed here different methods to determine the amount of nickel ejected in the explosion and see that values obtained are consistent with each other within errors.

4.6.2 Progenitor star properties

Litvinova & Nadëzhin (1985) investigated the course of SNe II by constructing hydrodynamical models. They investigated the dependence of SN outburst on three basic parameters: the ejected mass of the envelope (M_{ej}), the pre-SN radius (R_0) and the energy of explosion (E). Litvinova & Nadëzhin (1985) obtained approximate expressions for M_{ej}, R_0 and E in terms of three observational parameters: the plateau duration (t_p), the absolute V magnitude at the mid-plateau epoch (M_V) and the expansion velocity of the photosphere at the mid-plateau epoch (V_{ph}). Similarly, Popov (1993) derived somewhat different expressions for M_{ej}, R_0 and E based on the analytical models. The input parameters required in the model are the plateau duration (t_p), the photospheric velocity (V_{ph}) and the absolute magnitude (M_V).

The detailed photometric observations of SN 2004et show that the plateau length (t_p) was 110 ± 10 d and the absolute V magnitude (M_V) at the mid of the plateau is -17.08 ± 0.39. The spectroscopic observations of weak iron lines indicate a mid-plateau velocity (V_{ph}) of 3560 ± 100 km s^{-1} as reported by Sahu et al. (2006). We use the photospheric velocity given by Sahu et al. (2006) at the mid-plateau epoch for further analysis. Using the relations by Litvinova & Nadëzhin (1985) and Popov (1993) we derive the parameters M_{ej}, R_0 and E for SN 2004et which are listed in Table 4. The obtained estimates of M_{ej}, R_0 and E using expressions by Litvinova & Nadëzhin (1985) and Popov (1993) are consistent within errors.

If approximately $1.5\,M_\odot$ is enclosed in the neutron star and 0.5–$1.0\,M_\odot$ is lost by the wind, we obtain a range of roughly 10–20 $M_\odot$ for the progenitor of SN 2004et. Sahu et al. (2006) find that the [O I] luminosities of SN 2004et and SN 1987A are comparable. The [O I] luminosity of SN 1987A corresponds to an oxygen mass in the range 1.5–2 $M_\odot$. This oxygen mass corresponds to a main-sequence mass of 20 $M_\odot$ for SN 2004et. Li et al. (2005) derive the progenitor mass by analysing the high-resolution CFHT pre-SN images of NGC 6946 and suggest the progenitor to be a yellow supergiant of $15^{+5}_{-2}\,M_\odot$. Further details on the evolutionary sequence of the progenitor can be obtained from Li et al. (2005). The progenitors of SN IIP are generally considered to be red supergiants with thick hydrogen envelopes which give rise to the plateau phase in the optical light curve and a typical P-Cygni spectral profile. The spectroscopic analysis at 9 and 20 d after the explosion carried out by Li et al. (2005) shows a lack of a typical P-Cygni profile. Another interesting feature of SN 2004et to note here is the radio emission detected on 2004 October

05 (Stockdale et al. 2004) just 14 d after the explosion which clearly suggests the presence of dense circumstellar material. Therefore, it is likely that the progenitor experienced a red supergiant phase close to the time of explosion. Chevalier, Fransson & Nymark (2006) modelled the radio data and found a progenitor mass of $\sim20\,M_\odot$ for SN 2004et which includes the mass-loss rate obtained from radio observations. The measurements of the progenitor star by Li et al. (2005) were taken at ground-based resolution and it is possible that the star observed was blended with another star that did not partake in the explosion. The progenitor masses for SN 2004et obtained using different methods are consistent with the results within uncertainties. The light curves and the pre-SN radius 5 derived here suggests that the progenitor of SN 2004et is likely a red supergiant.

5 A COMPARISON WITH OTHER SN IIP

The light curves of SN 2004et are similar to those of typical type IIP supernovae SN 1999em and SN 1999gi during the plateau phase shown in Fig. 6. During the transition, the V-band light curve of SN 2004et matches well with SN 1999gi. Colour evolution of SN 2004et is studied in Fig. 8 and we see that the $U - B$ and $B - V$ colours of SN 2004et evolves slowly than that of SN 1999em. SN 2004et appears to be more like a normal type IIP apart from the difference in $U - B$ and $B - V$ colour evolution with SN 1999em. The spectrum of SN 2004et has a bluer continuum than SN 1999em (Li et al. 2005). The peculiar P-Cygni profile in Hα is dominated by the emission component unlike the typical P-Cygni profile in SN 1999em. SN 2004et evolves slower than SN 1999em in the ultraviolet part of the spectrum which explains the slow photometric evolution of $U - B$ and $B - V$ colours. Höflich et al. (2001) based on theoretical models find that though the peak luminosity varies among SN IIP, but the average absolute brightness during the plateau phase remains more or less the same with $\bar{M}_V \approx -17.6 \pm 0.6$ mag. In Fig. 12 we compare the absolute V-band light curves of SN 2004et
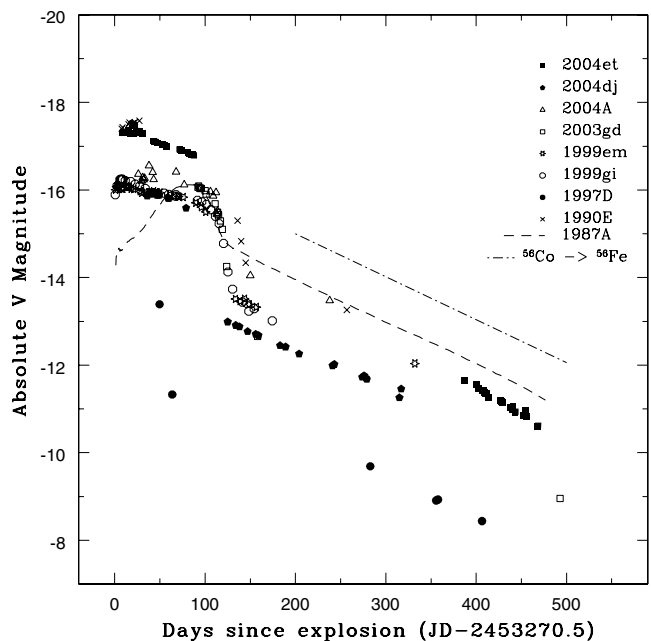

Figure 12. Comparison of absolute V-band light curves of SN 2004et, SN 2004dj, SN 2004A, SN 2003gd, SN 1999gi, SN 1999em, SN 1997D, SN 1990E and SN 1987A. The corresponding symbols representing each SN are shown in the figure. The magnitudes have been corrected for reddening and distance listed in Table 5.

Table 4. Progenitor star parameters.

	Ejected mass M_{ej} ($M_\odot$)	Pre-supernova radius R_0 ($R_\odot$)	Explosion energy E ($\times10^{51}$ erg)
Litvinova & Nadëzhin	16 ± 5	530 ± 280	0.98 ± 0.25
Popov	8 ± 4	1251 ± 937	0.60 ± 0.32

Table 5. Parameters of SN IIP sample.[a]

Supernova	Parent galaxy	Distance (Mpc)	A_V^{tot} (mag)	M^V (mag)	t_p (d)	E (10^{51}) (erg)	R($R_\odot$)	$M_{ejected}$ ($M_\odot$)	M_{ms} ($M_\odot$)	Estimated ^{56}Ni ($M_\odot$)
1987A	LMC	0.05	0.60		40	1.3	40	15	20	0.075
1990E	NGC 1035	21.0 ± 3	1.5	-16.93	131 ± 10	$3.4^{+1.3}_{-1.0}$	162^{+148}_{-78}	48^{+22}_{-15}		$0.073^{+0.018}_{-0.051}$
1997D	NGC 1536	13.43	0.07	-14.65	50	0.1	85	6 ± 1	8–12	0.002
1999em	NGC 1637	8.2 ± 0.6	0.31	-16.48	95	$1.2^{+0.6}_{-0.3}$	249^{+243}_{-150}	27^{+14}_{-8}	12 ± 1	$0.042^{+0.027}_{-0.019}$
1999gi	NGC 3184	11.1	0.65	-15.68	95	$1.5^{+0.7}_{-0.5}$	81^{+110}_{-51}	43^{+24}_{-14}	15^{+5}_{-3}	$0.018^{+0.013}_{-0.009}$
2003gd	M74	9.3 ± 1.8	0.43	-15.92	67^{+34}_{-25}			6	8^{+4}_{-2}	$0.016^{+0.010}_{-0.006}$
2004A	NGC 6207	20.3 ± 3.4	0.19	-16.24	80^{+25}_{-5}			11^{+10}_{-4}	9^{+3}_{-2}	$0.046^{+0.031}_{-0.017}$
2004dj	NGC 2403	3.47 ± 0.2	0.22	-15.88	100 ± 20	$0.86^{+0.89}_{-0.49}$	155^{+150}_{-75}	19^{+20}_{-10}	>20	0.02 ± 0.01
2004et	**NGC 6946**	**5.5 ± 1.0**	**1.27**	**− 17.08**	**110 ± 10**	**0.98 ± 0.25**	**530 ± 280**	**16 ± 5**	**∼20**	**0.06 ± 0.03**
2005cs	M51	8.4	0.34	-15.2	90–120				7–12	$\leqslant 10^{-2}$

[a]References: SN 1987A: Hamuy et al. (2003), Woosley, Hartmann & Pinto (1989); SN 1990E: Schmidt et al. (1993), Hamuy et al. (2003); SN 1997D: Turatto et al. (1998), Chugai & Utrobin (2000); SN 1999em: Leonard et al. (2002a), Hamuy et al. (2003); SN 1999gi: Leonard et al. (2002b), Hamuy et al. (2003); SN 2003gd: Hendry et al. (2005); SN 2004A: Hendry et al. (2006); SN 2004dj: Vinkó et al. (2006); SN 2004: The parameters for SN 2004et given in bold are from the present work (the progenitor star properties are those obtained from Litvinova & Nadëzhin (1985); SN 2005cs: Pastorello et al. (2006).

with those of SN 2004dj, SN 2004A, SN 2003gd, SN 1999em, SN 1999gi, SN 1997D, SN 1990E and SN 1987A. The parameters of these SNe along with references are mentioned in Table 5. The absolute *V*-band light curve of SN 2004et during the plateau phase matches very well with that of SN 1990E. The bolometric luminosities for these two SNe are similar during the plateau phase but the tail luminosity of SN 2004et is lower than that of SN 1990E. This is because of the lower ^{56}Ni mass synthesized during the explosion of SN 2004et as compared to SN 1990E.

Chevalier et al. (2006) place the SNe in two mass groups, 8–13 $M_\odot$ and 13–18 $M_\odot$, the low-mass and the high-mass group, respectively. The progenitor mass of different SNe IIP are listed in Table 5. There exist clearly two groups of SNe with high-mass progenitors (SN 1999em, SN 1999gi, SN 2004dj, SN 2004et) and low-mass progenitors (SN 1997D, SN 2003gd, SN 2004A, SN 2005cs). Thus, the progenitor of SN 2004et lies in the upper end of the mass range of SN IIP.

6 X-RAY EMISSION

We interpret the X-ray emission in terms of the circumstellar interaction model for type IIP SNe discussed by Chevalier et al. (2006) and references therein. The first two observations have temperatures above ∼5 × 10⁷ K (and the last is only slightly below this), a regime in which the reverse shock is expected to be non-radiative and free–free emission dominates. The X-ray luminosity is given by their equation (9), which comes from Fransson, Lundqvist & Chevalier (1996):

$$\frac{dL_{rev}}{dE} = 2 \times 10^{35} \zeta (n-3)(n-4)^2 T_8^{-0.24} e^{-0.116/T_8}$$

$$\times \left(\frac{\dot{M}_{-6}}{v_{w1}}\right)^2 V_{s4}^{-1} \left(\frac{t}{10\,d}\right)^{-1} \text{erg s}^{-1} \text{keV}^{-1},$$

where ζ is 0.86 for solar abundances, n is the index of the ejecta density profile [$\rho_{SN} = At^{-3}(r/t)^{-n}$], T_8 is the temperature in units of 10^8 K, $\dot{M}_{-6}$ is the mass-loss rate of the progenitor in units of $10^{-6}\,M_\odot\,\text{yr}^{-1}$, v_{w1} is the wind velocity in units of $10\,\text{km s}^{-1}$, V_{s4} is the shock velocity in units of $10^4\,\text{km s}^{-1}$, and t is the time since explosion.

Following the discussion of 2004et in Chevalier et al. (2006), we take $n = 10$ and use an expansion velocity of $15\,000\,\text{km s}^{-1}$ at 10 d (based on the maximum velocity of $14\,200\,\text{km s}^{-1}$ found by Li et al. 2005). The shock velocity is expected to evolve as $t^{-0.10}$ (Chevalier et al. 2006). The typical wind velocity for a yellow supergiant is not well known; red supergiants are expected to have winds with velocities of $10–15\,\text{km s}^{-1}$.

We use each of our three X-ray measurements to estimate the mass-loss of the progenitor, and find values of ($\dot{M}_{-6}/v_{w1}$) = 2.2, 2.1 and 2.5, respectively, assuming that the reverse shock is responsible for the X-ray emission. We can check the expected strength of the circumsteller shock using equation (8) of Chevalier et al. (2006). This predicts L_X (over the 0.5–8 keV band) of 2.9, 0.8 and 0.5 × 10^{36} erg s⁻¹, indicating that the reverse shock does indeed dominate.

However, there are some discrepancies between the data and this model. For example, the expected evolution of the total X-ray luminosity when free–free emission dominates as $L_X \propto t^{-1}$ (Chevalier & Fransson 1994), much different than the $t^{-0.4}$ evolution seen. One possibility is that the harder band (2–8 keV) X-ray emission is due to the reverse shock, and it shows roughly the expected evolution (Fig. 4). The softer band (0.5–2 keV) emission represents some (unexplained) steady component. Under this assumption, we calculate the mass-loss using only the 2–8 keV emission and find ($\dot{M}_{-6}/v_{w1}$) = 2.1, 1.8 and 2.0 for each of the three observations, respectively (again for $n = 10$). The temperature evolution is much more rapid than expected in the reverse shock model, in which $T \propto V_{s4}^2 \propto t^{-0.2}$ for $n = 10$ (Fransson et al. 1996). However, if there are

two distinct components of the emission (a steady soft component and a decaying hard component), these simple single-temperature models may be misleading. In addition, a single-temperature model of just the emitting shock region may be inaccurate (e.g. see the discussion in Nymark, Fransson & Kozma 2006).

A faster temperature evolution is expected for a smaller value of n, but even $n = 7$ results in a much slower evolution ($T \propto t^{-0.4}$) than is seen. However, if a smaller n is part of the explanation of the rapid temperature evolution, the mass-loss estimates would increase. For $n = 7$, we calculate $(\dot{M}_{-6}/v_{w1}) = 5.3$, 6.0 and 7.5 for each of the three observations, respectively.

7 RADIO EMISSION AT 1.4 GHZ

SN 2004et was detected at radio wavelengths by Stockdale et al. (2004) using the VLA on 2004 October 5.128 UT which is just ∼14 d after the explosion. It was extensively monitored at 22.5, 14.9, 8.46 GHz (Stockdale et al. 2004) and 4.99 GHz (Beswick et al. 2004). Chevalier et al. (2006) present the data in other frequencies along with the modelled light curve. We have the lowest frequency observation available here at 1.39 GHz using the GMRT.

Chevalier et al. (2006) have presented modelled light curves at different radio frequencies using two different combinations of ϵ_B and ϵ_r, where ϵ_B is the fraction of total blast wave energy in post shock magnetic field and ϵ_r that in relativistic particles. The two combinations are $\epsilon_B = 0.0013$, $\epsilon_r = 0.04$ and $\epsilon_B = 0.2$, $\epsilon_r = 0.001$. The details of the model can be obtained from Chevalier et al. (2006). We have scaled the radio light curves at different frequencies presented by Chevalier et al. (2006) to 1.39 GHz frequency. The scaled light curve obtained for 1.39 GHz for the two different combinations of ϵ_B and ϵ_r are shown in Fig. 13. We see that the observed flux at 1.39 GHz is close to that expected in both light curves, but it is in somewhat better agreement with that for the combination $\epsilon_B = 0.2$, $\epsilon_r = 0.001$.

Based on the 2–8 keV luminosity of X-ray observations adopting $n = 10$, we estimate a mass-loss rate for the progenitor star of ∼2 × 10^{-6} $M_\odot$ yr^{-1} for an assumed wind velocity of 10 km s^{-1} similar to the standard mass-loss prescription of $M_{-6} = 1.3$–3 for a progenitor
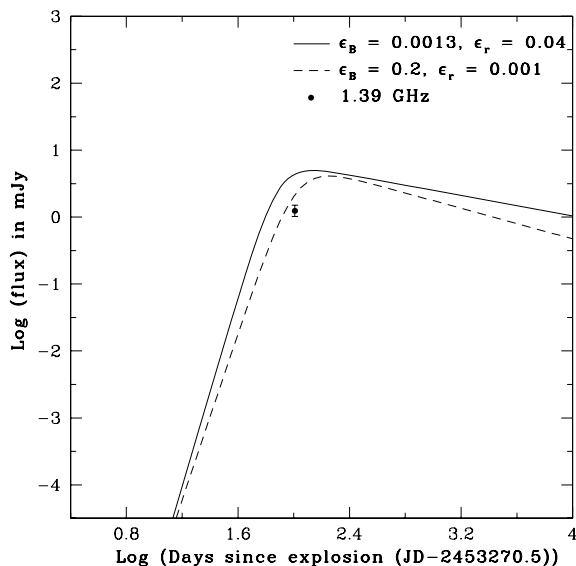

Figure 13. Observed radio data point of SN 2004et at 1.39 GHz compared to the model given by Chevalier et al. (2006) with two different combinations of ϵ_B and ϵ_r.

mass of 15 $M_\odot$. The value of $(\dot{M}_{-6}/v_{w1})$ is determined by the turn on time but it also depends on the temperature of the circumstellar medium (CSM). The radio model of Chevalier et al. (2006) lead to an estimate of $(\dot{M}_{-6}/v_{w1}) \approx 10 T_{cs5}^{3/4}$. With $(\dot{M}_{-6}/v_{w1})$ as determined from X-ray observations, we deduce that the temperature of the unshocked CSM is $T_{cs} \sim 10^4$ K.

8 CONCLUSIONS

The conclusions of the present paper are summarized below.

(i) We present the *Chandra* X-ray observations of a type IIP supernova SN 2004et at three epochs. We extract the X-ray spectra and try to fit two simple models – an absorbed power law and an absorbed mekal plasma model. We note that the spectrum softens with time. The X-ray luminosity is well characterized by $L_X \propto t^{-0.4}$.

(ii) An extensive photometric coverage starting from ∼ 14 to 470 d since explosion is presented. The explosion date is well constrained at 2004 September 22.0 (JD 245 3270.5) based on the pre-discovery magnitudes which is about 5 d before the discovery on 2004 September 27.0. SN 2004et showed a pronounced plateau phase with a plateau duration of ∼110 ± 10 d. The average absolute V magnitude during the plateau phase is −17.08. The light curves and colour curves of SN 2004et were compared with those of SN 1999em and SN 1999gi. The $U − B$ and $B − V$ colour evolution of SN 2004et is different than SN 1999em and they evolve slowly compared to SN 1999em.

(iii) Temporal evolution of photospheric radius and colour temperature is studied during the plateau phase using the technique by Hamuy et al. (2001). The temperature decreases from 12 100 to 5000 K with an increase in the photospheric radius.

(iv) The bolometric light curve of SN 2004et is constructed by integrating the flux in $UBVR_cI_c$ bands using a distance estimate of 5.5 ± 1.0 Mpc to NGC 6946 and the known reddening of $E(B − V) = 0.41 ± 0.07$. The tail bolometric luminosity was compared to that of SN 1987A.

(v) The ejected ^{56}Ni mass estimated in the explosion is 0.06 ± 0.03 $M_\odot$. The physical parameters such as the ejected mass (M_{ej}), the pre-SN radius (R_0) and the explosion energy (E) are estimated using the expressions given by Litvinova & Nadëzhin (1985) based on hydrodynamical models and those given by Popov (1993) based on the analytical models. This gives the ejected mass in the range 8–16 $M_\odot$ and a progenitor star of ∼20 $M_\odot$.

(vi) The radio observations at 1.4 GHz were carried out from GMRT. The 1.4-GHz observation was compared with the predictions of the model proposed by Chevalier et al. (2006). Thus, the model by Chevalier et al. (2006) reproduces and explains the light curve at 1.4 GHz, fairly.

(vii) The bulk of the X-ray emission detected by *Chandra* is due to a reverse shock. The 2–8 keV luminosity roughly follows the expected evolution of free–free emission from the reverse shock. The 0.5–2 keV luminosity stays roughly constant. Based on the 2–8 keV luminosity, we estimate a mass-loss rate for the progenitor star of ∼2 × 10^{-6} $M_\odot$ yr^{-1} for an assumed wind velocity of 10 km s^{-1}.

REFERENCES

Baars J. W. M., Genzel R., Pauliny-Toth I. I. K., Witzel A., 1977, A&A, 61, 99
Benetti S., Turatto M., Balberg S. et al., 2001, MNRAS, 322, 361
Bessell M. S., Castelli F., Plez B., 1998, A&A, 333, 231
Beswick R. J., Muxlow T. W. B., Argo M. K., Pedlar A., Marcaide J. M., 2004, IAUC, 8435
Broos P. S., Townsley L. K., Getman K., Bauer F. E., 2002, ACIS Extract, An ACIS Point Source Extraction, http://www.astro.psu.edu/xray/docs/TARA/ae_users_guide.html
Chevalier R. A., Fransson C., 1994, ApJ, 420, 268
Chevalier R. A., Fransson C., Nymark T. K., 2006, ApJ, 641, 1029
Chugai N. N., Utrobin V. P., 2000, A&A, 354, 557
Elmhamdi A., Chugai N. N., Danziger I. J., 2003, A&A, 404, 1077
Fransson C., Lundqvist P., Chevalier R. A., 1996, ApJ, 461, 993
Freeman P., Doe S., Siemiginowska A., 2001, in Starck J.-L., Murtagh F. D., eds, Proc. SPIE, Vol., 4477. p. 76
Hamuy M., Suntzeff N. B., González R., Martin G., 1988, AJ, 95, 63
Hamuy M., Pinto P. A., Maza J. et al., 2001, ApJ, 558, 615
Hamuy M., 2003, ApJ, 582, 905
Hendry M. A., Smartt S. J., Maund J. R. et al., 2005, MNRAS, 359, 906
Hendry M. A., Smartt S. J., Crockett R. M. et al., 2006, MNRAS, 369, 1303
Höflich P., Straniero O., Limongi M., Dominguez I., Chieffi A., 2001, Rev. Mex. Astron. Astrofis. Ser. Conf., 10, 157
Itagaki K., Yamaoka H., 2004, Int. Astron. Union Circ., 8413
Klotz A., Pollas C., Boer M., 2004, Int. Astron. Union Circ., 8413
Landolt A. R., 1992, AJ, 104, 340
Leonard D. C., Filippenko A. V., Gates E. L. et al., 2002a, PASP, 114, 35
Leonard D. C., Filippenko A. V., Li W. et al., 2002b, AJ, 124, 2490
Li W., Filippenko A. V., 2004, Int. Astron. Union Circ., 8413
Li W., Filippenko A. V., Van Dyk S. D., Cuillandre J.-C., 2004, Int. Astron. Union Circ., 8414
Li W., Van Dyk S. D., Filippenko A. V., Cuillandre J.-C., 2005, PASP, 117, 121
Lindberg H., 2004, http://www.astrosurf.com/snweb2/2004/04et/04etMeas.htm
Litvinova I. Y., Nadëzhin D. K., 1985, SVAL, 11, 145
Nymark T. K., Fransson C., Kozma C., 2006, A&A, 449, 171
Pastorello A., Zampieri L., Turatto M. et al., 2004, MNRAS, 347, 74
Pastorello A., Sauer D., Taubenberger S. et al., 2006, MNRAS, 370, 1752
Patat F., Barbon R., Cappellaro E., Turatto M., 1994, A&A, 282, 731
Pierce M. J., 1994, ApJ, 430, 53
Pooley D. et al., 2002, ApJ, 572, 932
Popov D. V., 1993, ApJ, 414, 712
Predehl P., Schmitt J. H. M. M., 1995, A&A, 293, 889
Rho J., Jarrett T. H., Chevalier R., 2007, CBET, 810
Sahu D. K., Anupama G. C., Srividya S., Muneer S., 2006, MNRAS, 372, 1315
Schlegel D. J., Finkbeiner P., Davis M., 1998, ApJ, 500, 525
Schmidt B. P., Kirshner R. P., Schild R. et al., 1993, AJ, 105, 2236
Schmidt B. P., Kirshner R. P., Eastman R. G., Phillips M. M., Suntzeff N. B., Hamuy M., Maza J., Aviles R., 1994, ApJ, 432, 42
Schoniger F., Sofue Y., 1994, A&A, 283, 21
Stockdale C. J., Weiler K. W., Van Dyk S. D., Sramek R. A., Panagia N., Marcaide J. M., 2004, Int. Astron. Union Circ., 8415
Suntzeff N. B., Bouchet P., 1990, AJ, 99, 650
Turatto M., Mazzali P. A., Young T. R. et al., 1998, ApJ, 498, L129
Van Dyk S. D., Garnavich P. M., Filippenko A. V., Höflich P., Kirshner B. P., Kurucz R. L., Challis P., 2002, PASP, 114, 1322
Vinkó J., Takáts K., Sárneczky K. et al., 2006, MNRAS, 369, 1780
Woosley S. E., Hartmann D., Pinto P. A., 1989, ApJ, 346, 395
Zwitter T., Munari U., Moretti S., 2004, Int. Astron. Union Circ., 8413

This paper has been typeset from a TEX/LATEX file prepared by the author.